Differentiation of apoptosis from necrosis by dynamic changes of reduced nicotinamide adenine dinucleotide fluorescence lifetime in live cells

Hsing-Wen Wang
Vladimir Gukassyan
National Yang-Ming University
Institute of Biophotonics
Taipei, Taiwan
E-mail: hwwang2@ym.edu.tw

Chien-Tsun Chen
Yau-Huei Wei
National Yang-Ming University
Institute of Biochemistry and Molecular Biology
Taipei, Taiwan

Han-Wen Guo
Jia-Sin Yu
Fu-Jen Kao
National Yang-Ming University
Institute of Biophotonics
Taipei, Taiwan

Abstract. Direct monitoring of cell death (i.e., apoptosis and necrosis) during or shortly after treatment is desirable in all cancer therapies to determine the outcome. Further differentiation of apoptosis from necrosis is crucial to optimize apoptosis-favored treatment protocols. We investigated the potential modality of using tissue intrinsic fluorescence chromophore, reduced nicotinamide adenine dinucleotide (NADH), for cell death detection. We imaged the fluorescence lifetime changes of NADH before and after staurosporine (STS)-induced mitochondria-mediated apoptosis and hydrogen peroxide (H_2O_2)-induced necrosis, respectively, using two-photon fluorescence lifetime imaging in live HeLa cells and 143B osteosarcoma. Time-lapsed lifetime images were acquired at the same site of cells. In untreated cells, the average lifetime of NADH fluorescence was ~1.3 ns. The NADH average fluorescence lifetime increased to ~3.5 ns within 15 min after 1 μM STS treatment and gradually decreased thereafter. The NADH fluorescence intensity increased within 15 min. In contrast, no significant dynamic lifetime change was found in cells treated with 1 mM H_2O_2. Our findings suggest that monitoring the NADH fluorescence lifetime may be a valuable noninvasive tool to detect apoptosis and distinguish apoptosis from necrosis for the optimization of apoptosis-favored treatment protocols and other clinical applications.
[DOI: 10.1117/1.2975831]

Keywords: nicotinamide adenine dinucleotide intrinsic florescence; two-photon fluorescence lifetime imaging; apoptosis detection, noninvasive optic probe; treatment outcome.

Paper 07476RR received Dec. 4, 2007; revised manuscript received Apr. 4, 2008; accepted for publication Apr. 18, 2008; published online Sep. 10, 2008.

1 Introduction

Cancer is among the world's leading causes of death. To improve the success rate of all cancer treatments including chemo, radiation, and photodynamic therapies, rapid and reliable readouts of treatment efficacy is in high demand. Direct monitoring of cell death, which is classically categorized into apoptosis and necrosis, is one way to measure treatment efficacy.[1] Preclinical and clinical studies have shown that the detection of apoptosis or cell death in general correlates with tumor response.[2–4] Specifically, monitoring of apoptosis can be useful in the design of apoptosis-favored treatment protocols, which could effectively kill target cells without inducing necrotic response, that have been preclinically demonstrated in the treatment of brain tumors using low dose photodynamic therapy.[5,6]

There is a range of noninvasive *in vivo* imaging/detection techniques to detect apoptosis such as magnetic resonance imaging (MRI) and spectroscopy, nuclear imaging [e.g., single-photon emission computed tomography and positron emission tomography (PET)], ultrasound, and optical imaging.[7] Molecular markers are generally used. The 40 kDa vesicle-associated protein, annexin V, is probably the most widely used apoptosis marker in molecular imaging. Radio-, (^{18}F)-, superparamagnetic iron oxide particles-, and fluorescence-labeled annexin V have been used in nuclear imaging,[4,8] PET,[9] MRI,[10] and optical imaging,[11] respectively. Caspases play a crucial role in the early phases of apoptosis and thus are the other apoptosis targets of molecular probes. Caspase 3-specific-cleavable reporter probe was used in luciferase-based bioluminescence imaging.[12] Besides molecular targeting, ultrasound measured the scattering power from tissues that showed changes due to nuclear condensation at the late stage of apoptotic process.[13] Diffusion MRI measured lipid droplets or apparent diffusion coefficient of water to indirectly monitor cell death.[14] Among these methods, ultrasound and diffusion MRI do not involve exogenous molecules and thus are clinically transferable. Diffusion MRI has been demonstrated to monitor therapeutic response in clinical

Address all correspondence to Hsing-Wen Wang, Institute of Biophotonics, National Yang-Ming University, 155 Li-Nong St., Sec. 2, Taipei 11221, Taiwan. Tel: 886-2-2826-7378; Fax: 886-2-2823-5460; E-mail: hwwang2@ym.edu.tw

1083-3668/2008/13(5)/054011/9/$25.00 © 2008 SPIE

trials.[14,15] Molecular targeting using radioactively labeled annexin V has been used to detect apoptosis in clinics although currently no clinical trial further evaluates its potential to assess the outcome of cancer therapy. Bioluminescence imaging is not readily transferable to clinical practice.

Mitochondria are known to be one of the key regulators in cell death particularly in apoptosis. Reduced nicotinamide adenine dinucleotide (NADH) is a key coenzyme in glycolysis and oxidative energy metabolism that acts as a principal electron and proton donor in mitochondria. It has also been widely accepted as a convenient noninvasive optical probe of metabolic state through the measurement of NADH fluorescence intensity.[16–18] Recently, the NADH fluorescence lifetime (τ) measurement has been used to monitor cell metabolic activities[19,20] based on (i) the lifetime changes of two major lifetime components (i.e., free NADH exhibiting a shorter lifetime, $\tau_1 \sim 0.4$ to 0.5 ns and bound NADH exhibiting a longer lifetime, $\tau_2 \sim 2$ to 3 ns) and (ii) the ratio of relative amplitudes of two major lifetime components. One advantage of NADH fluorescence lifetime measurement over intensity measurement is its sensitivity to the changes between free and bound form. The change in lifetime of NADH fluorescence from free to bound form differs as much as 10 times,[21–23] but the spectral shift of the NADH fluorescence from free to bound form is relatively small (~10 to 20 nm blueshift) as compared with the width of the NADH fluorescence spectrum (~150 nm).[20]

The aim of the present study was to investigate the potential of using the NADH lifetime measurement as a noninvasive probe of cell death. Similar to ultrasound and diffusion MRI methods, NADH signal is intrinsic so that it can be directly applied in a clinical setting once its utility of imaging cell death is demonstrated. Unlike ultrasound and diffusion MRI methods that indirectly probe cell death information based on cell morphological change (i.e., imaging nuclear condensation in ultrasound and cell swelling/shrinkage in diffusion MRI), NADH fluorescence lifetime method has a potential to detect the change of biochemical functions during cell death. We applied two-photon fluorescence lifetime imaging microscopy (FLIM) to map NADH fluorescence lifetime of unstained live HeLa cells and 143B osteosarcoma cells before and after treatment with staurosporine (STS) and hydrogen peroxide (H_2O_2). The STS-induced cell death has been well established to be executed by the mitochondria-mediated apoptotic pathway.[24–29]. High doses of H_2O_2 have been documented as a necrosis inducer.[30] Our results demonstrated that the average NADH fluorescence lifetime increased shortly after 1 μM STS treatment, but no significant lifetime change was observed after 1 mM H_2O_2 treatment of HeLa and 143B cells. These findings suggest that the average NADH lifetime changes may be a valuable indicator for apoptosis and for differentiation of apoptosis from necrosis of tissue cells in a noninvasive manner.

2 Materials and Methods

2.1 *Cell Cultures and Experiments*

Human osteosarcoma 143B and HeLa cells were cultured in Dulbecco's modified Eagle's medium (DMEM; Gibco, Invitrogen Corp., Carlsbad, California) containing 100 units/ml penicillin G, 100 μg/ml streptomycin sulfate, 0.5 μg/ml amphotericin B, and 5% fetal bovine serum (FBS) (Biological Industries, Kibbutz Beit Haemek, Israel) at 37 °C in a humidified atmosphere with 5% CO_2. At 24 h before fluorescence lifetime imaging and drug treatments, cells at a density of 2×10^4 cells/cm^2 were seeded onto 24 mm diameter round glass coverslips (Paul Marienfeld GmbH & Co., Lauda-Konigshofen, Germany) that had been coated with FBS. These coverslips were then kept in dishes and cultured in DMEM inside an incubator for 24 h. After 24 h, cells were completely attached onto the coverslip, ready to grow (in the early log phase of cell proliferation curve), and ready for fluorescence imaging. Immediately before fluorescence imaging, cells were washed twice using phosphate-buffered saline solution and then transferred to a cell chamber designed for viewing live cell specimens. A 1 mL aliquot of 5 mM HEPES (*N*-2-hydroxyethylpiperazine-*N*′-2-ethanesulfonic acid) buffer (5 mM KCl, 140 mM NaCl, 2 mM $CaCl_2$, 1 mM $MgCl_2$, 10 mM glucose, pH 7.4) was added into the cell chamber to nourish cells and to avoid light absorption of the red color of the culture medium. Fluorescence lifetime images of grouped cells were acquired at 1 to 3 sites per coverslip before treatment. The field of view (FOV) of each image was 100×100 μm. The FLIM system was equipped with a microscope cage incubator (Oko-lab, Naples, Italy) to maintain the optimal temperature during experiments. To optimize the NADH fluorescence intensity and to acquire high photon counts for statistical processing of the data, the imaging was conducted at room temperature (20 °C to 23 °C).[31] Additional measurements were performed at the physiological temperature (35 °C to 37 °C) in both controls and STS-treated cells to ascertain that the results of NADH lifetime measurements were not affected by the room temperature conditions.

Our previous experience with STS-induced apoptosis showed that the activation of caspase 3 occurred at 8 h or later after 25 nM STS treatment and the apoptotic bodies appeared at 24 h after treatment.[32] Maeno et al.[29] showed that the release of cytochrome *c* from mitochondria and the activation of caspase 3 occurred at ~2 to 4 h after 4 μM STS treatment of HeLa cells. Thus we randomly chose a medium dose (1 μM) of STS (Sigma-Aldrich, St. Louis, Missouri). Hydrogen peroxide is known to induce both apoptosis and necrosis depending on the concentration (e.g., 10 to 100μM for apoptosis, and 1 to 10 mM for necrosis) used.[30] We chose to use 1 mM H_2O_2 (Sigma-Aldrich) for necrosis induction. Time-lapsed fluorescence lifetime images were obtained at the same site (same FOV) before, immediately after (0 to 15 min), and up to 10 h after treatment with STS or H_2O_2. Controls are fluorescence lifetime images of cells without and before treatment.

2.2 *Caspase 3 Activity Assay*

Cells were disintegrated in 100 μl lysis buffer [12.5 mM Tris-HCl, 1 mM dithiothreitol, 0.125 mM ethylenediaminetetraacetic acid (EDTA), 5% glycerol, and an aliquot of complete protease inhibitor mixture (Roche Applied Sciences, Mannheim, Germany), pH 7.0] on ice for 30 min and centrifuged at 9000 *g* for 10 min at 4 °C. A 50 μg aliquot of protein was incubated with 20 μM Ac-DEVD-AFC (Calbiochem, San Diego, California), a fluorescent substrate of

caspase 3, in 500 μl of assay buffer [50 mM Tris-HCl, 1 mM EDTA, and 10 mM EGTA (ethyleneglycol-bis-(β-aminoethylether)-*N*, *N*, *N′*, *N′*-tetraacetic acid), pH 7.0] at 37 °C for 30 min in the dark. The fluorescence intensity was determined by spectrofluorometry (Hitachi F-3000, Tokyo, Japan) at an excitation wavelength of 380 nm and an emission wavelength of 508 nm as described previously.[32,33]

2.3 *NADH FLIM*

Time-domain FLIM was performed with a 60×1.45 numerical apenture PlanApochromat oil objective lens (Olympus Corp., Tokyo, Japan) on a modified two-photon laser scanning microscope (FV300 with the IX71 inverted microscope, Olympus Corp.) as described previously.[34] In this study, samples were excited at 750 nm (two-photon) by a mode-locked Ti:Sapphire Mira F-900 laser, pumped by a solid-state continuous wave 532 nm Verdi laser (both from Coherent Inc., Santa Clara, California). The scanning speed of the FV300 was controlled externally by a function generator (AFG310, Tektronix Inc., Beaverton, Oregon).

Fluorescence photons were detected in a non-descanned mode by a photon-counting photomultiplier (H7422P-40; Hamamatsu Photonics K.K., Hamamatsu, Japan). Time-resolved detection was conducted by the single-photon-counting SPC-830 printed circuit board (Becker & Hickl GmbH, Berlin, Germany). A bandpass filter of 450±40 nm (Edmund Optics Inc., Barrington, New Jersey) was inserted in the emission path for the detection of NADH that emits with the maximum at 450 nm.[35] Additional short pass and IR cut-off filters were used to reject reflected or scattered excitation light at 750 nm. The average laser power measured at the focal plane of the objective was ~3 to 5 mW, which was lower than the reported laser power of two-photon damage[36] and was found to be optimal for the prevention of photobleaching. All the images were taken at 256×256 pixels resolution with the acquisition time in the range of 900 to 1800 s for enough photon count statistics at the given laser power for further data analysis. To compare the emitted fluorescence intensity between controls and treated cells, we adapted the photon count from the peak time channel (and with fixed binning parameters) of the recorded decay curve at the brightest point of a FLIM image.

2.4 *FLIM Data Analysis*

Data were analyzed with the commercially available SPCImage version 2.8 software package (Becker & Hickl GmbH) via a mathematical convolution of a model function and the instrument response function (IRF), and fitting to the experiment data. To calculate the lifetime from the composite decays of NADH, we convolved an IRF, I_{instr}, with a double-exponential model function, defined in Eq. (1), with offset correction for the ambient light and/or dark noise I_0 to obtain calculated lifetime decay function $I_c(t)$ in Eq. (2)

$$F(t) = a_1 e^{-t/\tau_1} + a_2 e^{-t/\tau_2}, \tag{1}$$

$$I_c(t) = \int_{-\infty}^{\infty} I_{\text{instr}}(t)\{I_0 + F(t)\}\mathrm{d}t. \tag{2}$$

Here, $a_1 e^{-t/\tau_1}$ and $a_2 e^{-t/\tau_2}$ represent the contributed fluorescence decays from free and bound NADH, respectively; τ_1 and τ_2 represent their corresponding lifetimes; and a_1 and a_2 are the corresponding relative amplitudes. I_{instr} was calculated automatically by SPCImage from the rising edge of the fluorescence decay.

The model parameters (i.e., a_i and τ_i) were derived by SPCImage software by fitting the calculated decay $I_c(t_k)$, defined in Eq. (2), to the actual data $I_a(t_k)$ through minimizing the goodness-of-fit χ_R^2 function defined in Eq. (3) using the Levenberg-Marquardt search algorithm

$$\chi_R^2 = \left[\sum_{k=1}^{n} [I(t_k) - I_c(t_k)]^2 / I(t_k)\right] \Big/ (n-p). \tag{3}$$

Here n is the number of the data (time) points (equal to 256 in this study), and p is the number of the model parameters.[37]

3 Results

3.1 *NADH Fluorescence Intensity and Lifetime Images of Intact Cells*

Figure 1 shows representative images, fitting curves, and lifetime distribution from control 143B cells. It includes a fluorescence intensity image [Fig. 1(a)], fluorescence lifetime image [Fig. 1(b)] using two-photon FLIM, the corresponding fluorescence decay curves (measured: blue; fit: red), the fitting residuals [Fig. 1(c)], and normalized lifetime histograms [Fig. 1(d)] of the 256×256 lifetime image as shown in Fig. 1(b). This entire image was acquired over a period of 1300 s. In control cells, the average photon count collected over the given period of time was approximately 600 in the peak time channel.

Figure 1(a) shows that the fluorescence signals in the cytoplasm displayed punctuate perinuclear patterns, which were attributed to mitochondria-associated NADH.[19,38] No fluorescence was seen in the nuclei or on the nuclear membrane. In Fig. 1(b), each pixel represents the average lifetime (τ_{ave}) of the short (τ_1) and the long (τ_2) lifetime components weighted by their relative contributions a_1 and a_2, respectively, such that $\tau_{\text{ave}}=(a_1\tau_1+a_2\tau_2)/(a_1+a_2)$. The scale of the color mapping was chosen for later comparison with FLIM images of treated cells so that the blue color represents the longer lifetime (maximum 4000 ps) and the red color presents the shorter lifetime (minimum 200 ps). Overall, the NADH fluorescence in the control 143B cells exhibited an average lifetime (τ_{ave}) of ~1300 ps, which corresponds to the yellowish color in the selected color scale. The lifetime across the entire FOV or even within a single cell was not homogeneous: some pixels tend to be greenish and some tend to show orange color. Figure 1(c) demonstrates the fitting curve obtained from Fig. 1(b), with the goodness-of-fit residuals shown in the bottom panel of Fig. 1(c). Finally, the distribution of the averaged lifetime (τ_{ave}) from all pixels shown in Fig. 1(b) is presented in Fig. 1(d), which depicts the normalized histogram (H_{norm}) of τ_{ave}. The histogram shows a peak (τ_{peak}) at ~1300 ps with a full width at half maximum ~500 ps. This

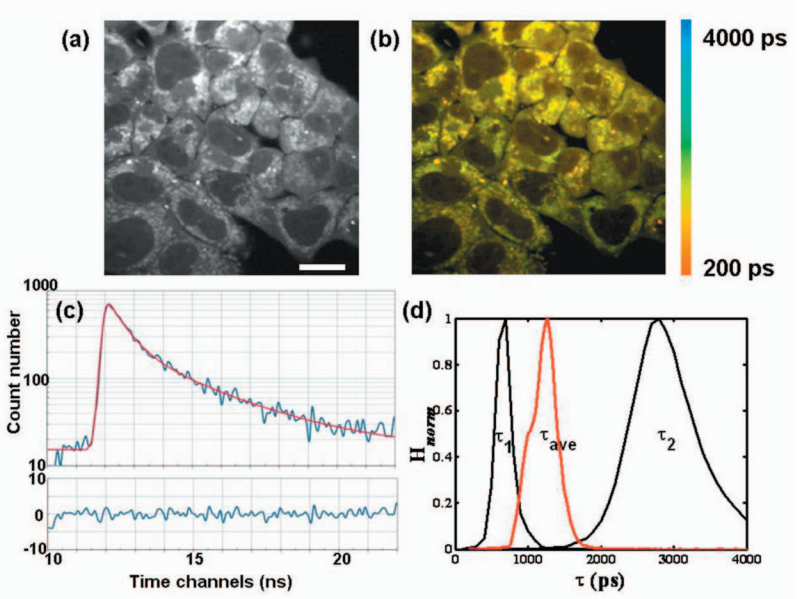

Fig. 1 Measurement of the intensity and average lifetime of NADH fluorescence in 143B cells. The intensity and average lifetime images of NADH fluorescence in 143B cells are shown in gray (a) and color scale (b), respectively, using two-photon FLIM with the excitation wavelength at 750 nm. The FOV of each image is 100×100 μm. The scale bar in (a) is 20 μm. A representative fluorescence lifetime decay curve (blue curve in the top panel), the fit (red curve in the top panel), and the residuals (bottom panel) are shown (c). The normalized histograms over the 256 x 256 pixel lifetime image shown in (b) were plotted for τ_1, τ_2, and τ_{ave} (d).

broad distribution illustrates the inhomogeneous color distribution observed in Fig. 1(b). To compare with previously published results regarding the values of the NADH short (τ_1) and long (τ_2) lifetime components, we obtained τ_1 and τ_2 from the entire image pixels by SPCImage software and plotted their normalized histogram in the same figure [Fig. 1(d)]. The histograms of τ_1 and τ_2 showed peaks at ~600 and ~3000 ps, respectively. These results are close to the previously published lifetime values of free (~400 to 500 ps) and bound NADH (~2000 to 3000 ps).[22,23] The observation that τ_2 had a broader distribution than τ_1 may be attributed to the wide distribution of lifetimes of NADH molecules bound to different proteins.[39,40]

We acquired NADH lifetime images from a total of 35 sites of control HeLa cells (from 15 coverslips) and 11 sites of control 143B osteosarcoma cells (from 8 coverslips). The values of τ_{peak} from all of the lifetime images were analyzed, recorded, and averaged. Table 1 summarizes the total number of sites (N_{site}) and the corresponding mean ± standard error (SE) of the τ_{peak} values from control HeLa cells and control 143B cells. The results showed that HeLa and 143B cells had the average τ_{peak} values equal to 1360 ± 24 (N=35) and 1260 ± 49 ps (N=11), respectively. The two mean values are not significantly different as judged by two-tailed Student's t test (p value=0.09). The mean value of all control τ_{peak} values is 1336 ± 22 ps, which will be used later in Figs. 4 and 6 for comparison.

3.2 *Cell Morphological Change and Caspase 3 Activation Confirmed STS-Induced Apoptosis and H_2O_2-Induced Necrosis*

Although STS-induced apoptosis and high dose H_2O_2-induced necrosis have been well documented, we observed the cell morphology and measured caspase 3 activity to confirm the cell death pathway at the drug dose we chose. Figure 2(a) shows the light microscopic images of HeLa cells 15 min and 5 h after either H_2O_2 or STS treatment. All the images were taken at the same magnification. Cell swelling or eruption, a typical feature when cells are under necrotic pathway, was observed in both 15 min and 5 h after H_2O_2 treatment. In contrast, the typical feature of apoptotic cells, cell shrinkage,

Table 1 Summary of the number of sites (N_{site}) of NADH lifetime images acquired from the number of coverslips ($N_{coverslip}$) in control, STS-treated, and H_2O_2-treated cells. The number of sites is the same as the number of coverslips in treated cells because of time sequence measurements at the same site. The corresponding means (±SE) of the peaks (τ_{peak}) of the average lifetime (τ_{ave}) distributions were calculated and listed with the unit of picoseconds (ps). τ_{peak} was defined as the peak position (or the maximal value) of the τ_{ave} histogram from each 256×256 pixel lifetime image. For STS-treated cells, only the lifetime at the first time point (0 to 15 min) was listed. For H_2O_2-treated cells, the lifetimes at both 0 to 15 and 0 to 25 min after treatments (N_{site} at each time point is 2) were averaged and listed to account for a larger number of the samples for averaging.

Cells		Controls	0 to 15 Min After STS Treatment	0 to 25 Min After H_2O_2 Treatment
HeLa	N_{site} ($N_{coverslip}$)	35 (15)	6 (6)	4 (4)
	Mean±SE	1359±24	3570±56	1514±51
143B	N_{site} ($N_{coverslip}$)	11 (8)	5 (5)	N/A
	Mean±SE	1260±49	3448±76	N/A

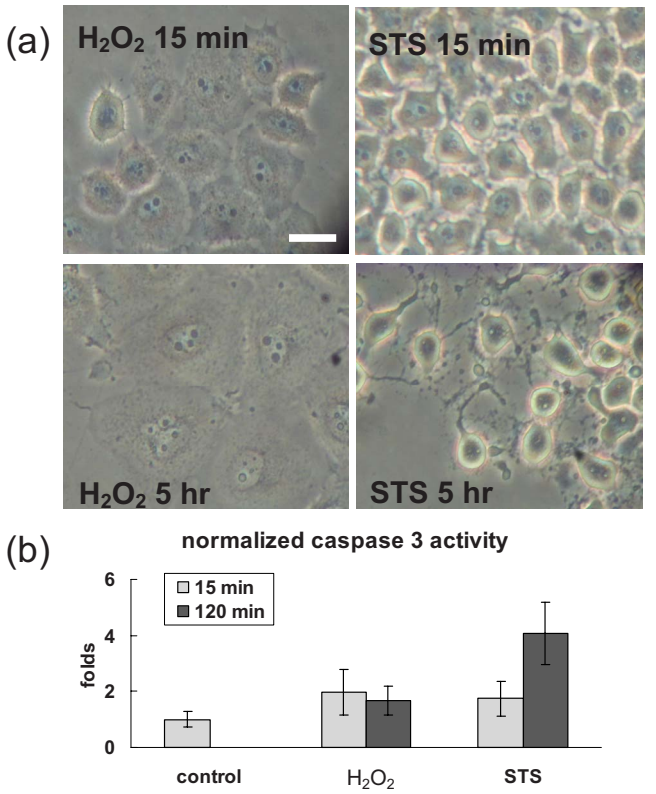

Fig. 2 The morphology (a) and normalized caspase 3 activity (b) of HeLa cells after treatment with H_2O_2 and STS, respectively. The FOV of each image is 180×180 μm. The scale bar in (a) is 30 μm.

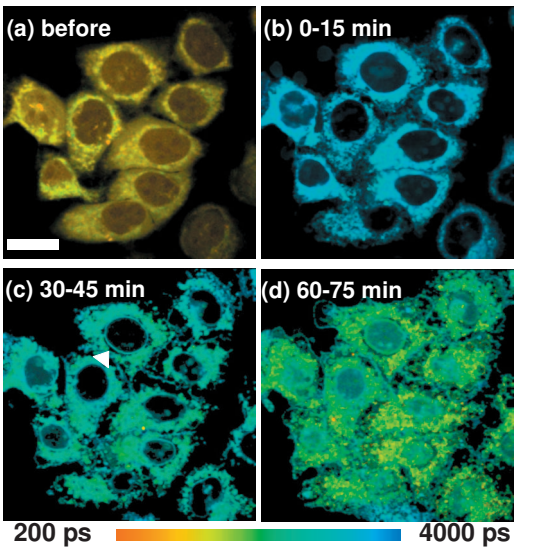

Fig. 3 Effect of staurosporine treatment on the FLIM images of HeLa cells. The FLIM images of HeLa cells from the same sites before (a), 0 to 15 min (b), 30 to 45 min (c), and 60 to 75 min (d) after treatment with 1 μM STS. The FOV of each image is 100×100 μm. The scale bar in (a) is 20 μm.

was observed in STS-treated cells. Figure 2(b) shows the normalized caspase 3 activities of HeLa cells before (controls), 15 min after, and 2 h after either H_2O_2 or STS treatment. Caspase 3 activity was significantly higher at 2 h after STS treatment compared with controls, indicating that STS-treated cells were undergoing apoptosis. However, no significant increase of caspase 3 activity was observed in cells at 15 min or 2 h after H_2O_2 treatment.

3.3 *NADH Fluorescence Lifetime Increased Immediately after STS-Induced Apoptosis*

Figure 3 shows the representative FLIM images (in color mapping) before, 0 to 15, 30 to 45, and 60 to 75 min after 1 μM STS treatment at the same FOV of HeLa cells. All the figures are displayed using the same scale of color bar as in Fig. 1(b) that the minimal and maximal lifetime is 200 ps (red) and 4000 ps (blue), respectively. Similar to Fig. 1(b), control HeLa cells [Fig. 3(a)] had $a\sim$1300 ps lifetime (yellowish image in the selected color scale). The acquisition time of this control image was 900 s or 15 min. Immediately after STS treatment, we continuously acquired FLIM images with the acquisition time of 15 min per image for up to 90 min (the images acquired at 15 to 30, 45 to 50, and 75 to 90 min after treatment are not shown) at the same site to trace the response of the specimen. Apparently, the color-coded lifetime image exhibited blueshift (increased lifetime) at 0 to 15 min [Fig. 3(b)] after treatment, and then exhibited redshift at 60 to 75 min [Fig. 3(d)]. The nuclear areas tended to decrease in size with the increment of treatment time. A ringlike structure surrounding the nucleus [arrow head in Fig. 3(c)] was observed. In addition, the overall intensity of NADH fluorescence significantly increased immediately after STS treatment so that the laser power was decreased to escape the photomultiplier tube saturation. The recorded average photon count for the STS-treated cells was more than 1000, approximately twice higher than that in controls (600 counts), in the peak time channel of the recorded decays.

The distributions of the average lifetime (τ_{ave}) [Figs. 3(a)–3(d)] were plotted on the top panel of Fig. 4. The curve labels (a) to (d) correspond to the results of Figs. 3(a)–3(d), respectively. An immediate lifetime increase after STS treatment was observed that the histogram shifted from the lower lifetime [curve (a)] to the higher lifetime [curve (b)] values. Then, the lifetime decreased and the histogram shifted toward the controls and became broader. The peak (i.e., maximal) value of τ_{ave} histograms, τ_{peak}, increased from $\sim$1300 ps [controls, curve (a)] to $\sim$3500 ps at 0 to 15 min after STS treatment [curve (b)], and then decreased to $\sim$2200 ps at 60 to 75 min.

Similar results were repeatedly observed in a total of 6 sites (6 coverslips) of HeLa cells and 5 sites (5 coverslips) of 143B cells and are summarized in the bottom plot of Fig. 4. Here the number of sites is the same as the number of coverslips because time sequence measurements were performed at the same site of cells. The bottom panel of Fig. 4 plotted the mean and standard error (SE) of the τ_{peak} at all time points over all STS-treated HeLa and 143B cells. The number of sites acquired was decreased as a function of time and was labeled below each data point in the figure. The time point was assigned as the mean value of the acquisition period of time. For example, 7.5 min represents the data point acquired at 0 to 15 min after treatment, except that the latest point was

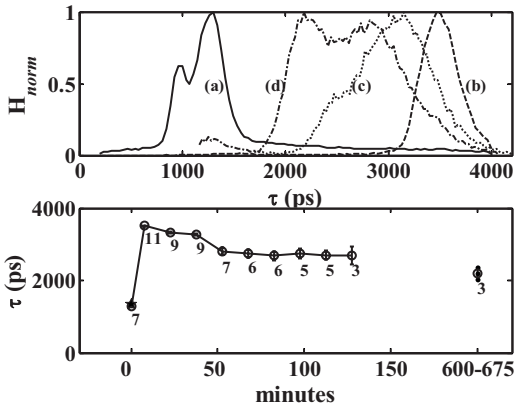

Fig. 4 Effect of staurosporine treatment on the distributions of the average lifetime (τ_{ave}) of the FLIM images of HeLa and 143B cells. The top panel shows the plot of the distributions of the average lifetime (τ_{ave}) corresponding to the FLIM images in Figs. 3(a)–3(d). The bottom panel shows the plot of the mean and standard error (SE) of the τ_{peak} as the function of time in all STS-treated cells. The number of sites acquired at each time point was labeled below each data point. The mean τ_{peak} value (±SE) of controls (i.e., 1336±22 ps) was plotted (star) in the same figure.

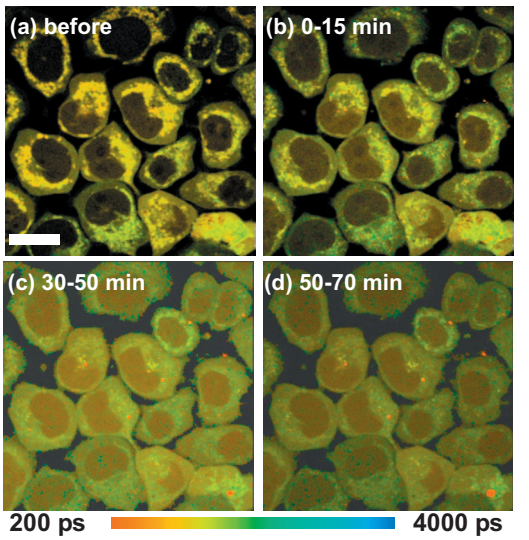

Fig. 5 Effect of H_2O_2 treatment on the FLIM images of HeLa cells. The FLIM images of HeLa cells were recorded from the same sites before (a), 0 to 15 min (b), 30 to 45 min (c), and 45 to 60 min (d) after treatment of the cells with 1 mM H_2O_2. The FOV of each image is 100×100 μm. The scale bar in (a) is 20 μm.

labeled as 600 to 675 min. The mean τ_{peak} value (±SE) of all controls (i.e., 1336±22 ps) was plotted (star) in the same figure for comparison. The mean τ_{peak} values (±SE) for HeLa and 143B cells at 0 to 15 min after STS treatment are listed in Table 1. The mean τ_{peak} values at 0 to 15 min after STS treatment for HeLa or 143B cells are significantly different from those values of the controls (p value=1.4×10^{-16}). The two mean values of HeLa and 143B cells (i.e., 3570±56 versus 3448±76) are not significantly different (p value =0.23).

3.4 *No NADH Fluorescence Lifetime Change in High Dose H_2O_2-Induced Necrosis*

Figure 5 shows the representative FLIM images (in the same color mapping as previous FLIM images of controls and STS-treated cells) before, 0 to 15, 30 to 50, and 50 to 70 min after treatment with 1 mM H_2O_2, taken from the same FOV of HeLa cells. In contrast to the FLIM images of STS-treated cells shown in Fig. 3, all images in Fig. 5 tend to be yellowish in the same selected color scale, which indicates that there was no significant lifetime change after H_2O_2 treatment. The fluorescence intensity or photon counts tended to decrease after H_2O_2 treatment [as seen in the changes of signal-to-background noise from Figs. 5(a)–5(d)], which in part is due to the NADH oxidation[16] by H_2O_2. The recorded average photon count for the H_2O_2-treated cells was ~100 to 200 (i.e., 3 to 6 times lower than that of controls) in the peak time channel.

The top panel of Fig. 6 plotted the normalized histogram of τ_{ave} of NADH lifetime images shown in Figs. 5(a)–5(d). The curves (b) to (d) overlapped with one another. There is slight difference between curve (a) and curves (b) to (d). Similar to the bottom panel of Fig. 4, the bottom panel of Fig. 6 plotted the mean error and standard error of the τ_{peak} at all time points over all H_2O_2-treated HeLa cells. The time point was assigned the same way as in Fig. 4 except the latest time point labeled as 135 to 185 min. The mean τ_{peak} value (±SE) of controls (i.e., 1336±22) was plotted (star) in the same figure for comparison. The number of sites acquired at each time point was labeled below each data point in the figure. We observed no significant difference in τ_{peak} at all time points. To get more data points for averaging and comparing with the results of controls and apoptotic cells in Table 1, the mean τ_{peak} values (±SE) for both time points at 0 to 15 min (N =2) and 0 to 25 min (N=2) after treatment were calculated and listed in Table 1. The mean τ_{peak} values at 0 to 25 min after H_2O_2 treatment in HeLa cells are marginally different from the values of control HeLa cells (p value=0.05).

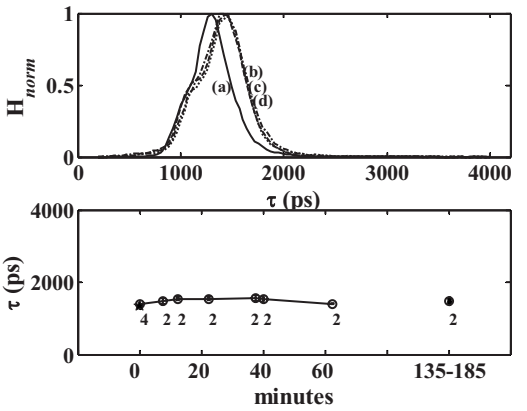

Fig. 6 Effect of H_2O_2 treatment on the distributions of the average lifetime (τ_{ave}) of the FLIM images of HeLa cells. The top panel plotted the distributions of the average lifetime (τ_{ave}) corresponding to the FLIM images in Figs. 5(a)–5(d). The bottom panel plotted the mean and standard error (SE) of the τ_{peak} as a function of time in all H_2O_2-treated cells. The number of sites acquired at each time point was labeled below each data point. The mean τ_{peak} value (±SE) of the controls (i.e., 1336±22 ps) was plotted (star) in the same figure.

Table 2 The NADH lifetime acquired under physiological condition and using short image acquisition time (100 s), respectively, in control and STS-treated cells. The corresponding means (±SE) of the peaks (τ_{peak}) of the average lifetime (τ_{ave}) distributions were calculated and listed with the unit of picoseconds (ps). τ_{peak} was defined as the peak position (or the maximal value) of the τ_{ave} histogram from each 256×256 pixel lifetime image. For STS-treated cells, only the lifetime at the time point 0 to 15 min was listed.

		Controls		0 to 15 Min After STS Treatment	
Cells		Physiology	Short Image Acquisition	Physiology	Short Image Acquisition
HeLa	Mean±SE (N_{site})	1306±91 (4)	1396±17 (4)	3544±103 (3)	3402±83 (4)
143B	Mean±SE (N_{site})	1192 (1)		3545±31 (3)	

4 Discussion

In live cells, NADH, reduced NADH phosphsate (NADPH), and flavins [or flavin adenine dinucleotide (FAD)] are intrinsic fluorophores that have sufficient concentration to yield detectable fluorescence signals under two-photon excitation at 740 nm.[39] The flavin signals that emit fluorescence maxima at ~550 nm can be spectrally separated from NAD(P)H signals that emit fluorescence maxima at ~450 nm. Although NADH and NADPH have nondiscriminating spectral features,[41] NADH dominates the intrinsic fluorescence of live cells because the contribution of NADPH to the intrinsic fluorescence is small[42] and the quantum yield of mitochondrial NADH is 1.25 to 2.5 times higher than that of NADPH.[43] In this study, we used a 450±40 nm bandpass emission filter to selectively collect the NADH fluorescence signals, although we used two-photon excitation at 750 nm, instead of 740 nm used in other published studies, due to our instrument limitation. Recently, Wu et al.[20] reported that increase of flavin fluorescence contributed to both lifetime components (τ_1 and τ_2) and the ratio of the corresponding amplitudes (a_1/a_2) in the fluorescence decay when the single photon excitation wavelength increased from 365 to 405 nm (equivalent to wavelengths from 730 to 810 nm in two-photon excitation) and when a 10 nm bandpass emission filter (λ_{em}=447 to 457 nm) was used. In their study, the τ_1, τ_2, and a_1/a_2 of control SiHa cells were found to change, not consistently increase or decrease, ~6% to 12%. However, Skala et al.[44] showed that there was no measurable fluorescence at 900 nm excitation, which is optimal for the two-photon excitation of flavins,[35] with their two-photon FLIM system, neither did FAD contribute to their observed lifetime at 780 nm excitation in the hamster cheek pouch. Thus, we concluded that the flavin fluorescence contribution to our results using two-photon excitation wavelength at 750 nm was negligible.

To confirm that the difference in lifetime changes between controls and STS and H_2O_2 treatments is not due to long image acquisition time (~15 to 20 min) and/or room temperature condition, we performed additional FLIM measurements using shorter acquisition time (5 to 10 min) and/or at the physiological temperature maintained in the microscope cage incubator (35°C to 37°C). Similar results of the NADH lifetime values, with lower photon counts and thus noisier τ_{ave} histogram plots, have been observed using 100 s to 10 min acquisition times in controls, STS-treated, and H_2O_2-treated cells (data not shown). Table 2 lists the NADH lifetime acquired under physiological condition and using short image acquisition time (100 s), respectively, in control and STS-treated cells. From 4 measurements of HeLa cells taken using shorter acquisition time (100 s), lifetime increased from 1396±17 ps before to 3402±83 ps at 0 to 15 min after treatment. From measurements of both HeLa (N_{site}=3 to 4) and 143B (N_{site}=1 to 3) cells taken at the physiological temperature, we observed the same trends of changes in lifetime and intensity in STS-treated cells including increased τ_{ave} from 1306±91 (HeLa) and 1165 (143B) ps before to 3544±103 (HeLa) and 3545±31 (143B) ps at 0 to 15 min after treatment, decreased τ_{ave} thereafter, increased NADH fluorescence intensity after treatment (indicated by using lower input laser power and detecting higher photon counts after STS treatment), shrinkage of nuclei, and the appearance of perinuclear rings [arrowhead in Fig. 3(d)].

Similar results of increased NADH fluorescence intensity were reported by Levitt et al.[45] and by Liang et al.[46] Levitt et al.[45] observed that intense fluorescence was progressively confined to a gradually smaller perinuclear cytoplasmic region in the cells that had been treated with cisplatin. Their results suggest that this strongly fluorescent, highly metabolically active perinuclear ring represents a subpopulation of mitochondria that are mobilized in response to the apoptotic stimulus and may provide the energy required to execute the final step of apoptosis.

The increase in the average lifetime of NADH fluorescence after STS-induced apoptosis (Fig. 3) may be attributed to two possible mechanisms based on the lifetime distribution analysis. One mechanism is that the portion of bound NADH to total amounts of NADH is higher than that of free NADH [i.e., $a_2/(a_1+a_2) > a_1/(a_1+a_2)$ such that $\tau_{ave}=(a_1\tau_1+a_2\tau_2)/(a_1+a_2)$ increased] assuming their lifetimes (i.e., τ_1 and τ_2) remain the same. The other mechanism is that the bound NADH lifetime τ_2 increases, assuming that the free NADH lifetime τ_1 does not change, due to microenvironment changes that NADH binds to different enzymes during apoptosis. We examined the histograms of τ_1 and τ_2 in several FLIM images of STS-treated cells at all time points and found that both mechanisms are possible (data not shown). For example, at 0 to 15 min after STS treatment, the histogram of τ_1, τ_2, and

τ_{ave} are almost identical [curve (b) in Fig. 4] that single exponential fit was applicable in this case. This indicates that all free NADH (i.e., the short lifetime component) became a bound form (i.e., the long lifetime component). At later time points after STS treatment, some τ_2 histograms became broader (in both longer and shorter lifetime directions), which indicates that some NADH may bind to different enzymes to broaden the lifetime distribution. Vishwasrao et al.[39] reported three types of enzyme-bound NADHs using four component analyses in hippocampal slices. They found that the ratio between free NADH and individual enzyme-bound species of NADH changed significantly under hypoxia, which indicates a redistribution of the protein-bound NADH to enzyme binding sites.

The STS-induced apoptotic pathway has been well established to be due to internal signals and involve mitochondrial membrane potential ($\Delta\Psi$) change, cytochrome *c* release, caspase 3 activation, and production of reactive oxygen species.[24–26] In this study, we observed increased NADH fluorescence lifetime at relatively early time points (within 15 min after 1 μM STS treatment) as compared with the activation of caspase 3 at 2 h after 1 μM STS treatment [Fig. 2(b)] and cytochrome *c* release and the caspase 3 activation at ~2 to 4 h after higher dose (4 μM) STS treatment as described in the study by Maeno et al.[29] Thus we have hypothesized that the immediately increased NADH lifetime may be related to early apoptotic activities. Annexin V was used to indicate early apoptosis[47,48] to stain the exposure of phosphatidylserine (PS) on the external leaflet of the plasma membrane. We performed annexin V fluorescence imaging (data not shown) and observed that annexin V binding, quantified by averaging binding percentages over five different 100 $\times$ 100 μm FOVs, appeared at 15 min after 1 μM STS treatment (binding percentage $<2\%$). The binding percentage increased as time increased to be ~4% and ~50% at 1 h and 5 h after STS treatment, respectively. Lugli et al.[48] showed that the appearance of PS exposure (annexin V–positive) was correlated to intermediate $\Delta\Psi$ in quercetin-induced apoptosis of U937 cells, which could be important to maintain adenosine triphosphate (ATP) production for the activation of caspases and induction of cell death. Halestrap et al.,[49,50] showed that the mitochondrial permeability transition pore (MPTP) opening can be transient and thus does not cause ATP depletion, and then the cell dies by apoptosis. If the MPTPs stay open, ATP is depleted and the cells die by necrosis.[50] Furthermore, it was demonstrated that the cytosolic ATP level was increased in HeLa cells immediately after treatment with 4 μM STS.[51] It remains unclear whether our observations that NADH lifetime increased shortly after apoptosis and NADH redistribution are related to NADH binding to different proteins in mitochondria for more efficient generation of ATP in the target cells. Further studies are needed to reveal the relationship between NADH lifetime dynamics, mitochondrial membrane potential, MPTP opening, and ATP production/maintenance in the early phase of apoptosis.

5 Conclusions

Nicotinamide adenine dinucleotide is a principal electron and proton donor in mitochondria, which are known to be one of the key regulators in cell death particularly in apoptosis. We have demonstrated that NADH fluorescence lifetime significantly changed immediately after 1 μM STS-induced apoptosis, but not 1 mM H_2O_2-induced necrosis in HeLa and 143B osteosarcoma cells. This increased lifetime was in the early phase of apoptosis and was in part due to NADH redistribution from free to bound form in mitochondria possibly for more efficient generation of ATP in the target cells. Our findings suggest that the NADH lifetime changes may be a valuable noninvasive marker for the detection of apoptosis.

Acknowledgments

We acknowledge the imaging core facility of National Yang-Ming University, Professor Der-Ming Yang who provided culture chamber, and Professors Britton Chance, Chi-Hung Lin, and Arthur Chiou for valuable discussions. This work was supported by a new faculty start-up fund from National Yang-Ming University, the "Aim for Top University Plan" from the Ministry of Education of Taiwan, and Grant Nos. NSC 94-2321-B-010-004-YC and NSC 95-2112-M-010-002 from the National Science Council of Taiwan.

References

1. M. F. Corsten, L. Hofstra, J. Narula, and C. P. Reutelingsperger, "Counting heads in the war against cancer: defining the role of annexin A5 imaging in cancer treatment and surveillance," *Cancer Res.* **66**(3), 1255–1260 (2006).
2. T. A. Buchholz, D. W. Davis, D. J. McConkey, W. F. Symmans, V. Valero, A. Jhingran, S. L. Tucker, L. Pusztai, M. Cristofanilli, F. J. Esteva, G. N. Hortobagyi, and A. A. Sahin, "Chemotherapy-induced apoptosis and Bcl-2 levels correlate with breast cancer response to chemotherapy," *Cancer J.* **9**(1), 33–41 (2003).
3. B. Dubray, C. Breton, J. Delic, J. Klijanienko, Z. Maciorowski, P. Vielh, A. Fourquet, J. Dumont, H. Magdelenat, and J. M. Cosset, "*In vitro* radiation-induced apoptosis and early response to low-dose radiotherapy in non-Hodgkin's lymphomas," *Radiother. Oncol.* **46**(2), 185–191 (1998).
4. T. Belhocine, N. Steinmetz, R. Hustinx, P. Bartsch, G. Jerusalem, L. Seidel, P. Rigo, and A. Green, "Increased uptake of the apoptosis-imaging agent (99m)Tc recombinant human Annexin V in human tumors after one course of chemotherapy as a predictor of tumor response and patient prognosis," *Clin. Cancer Res.* **8**(9), 2766–2774 (2002).
5. S. K. Bisland, L. Lilge, A. Lin, R. Rusnov, and B. C. Wilson, "Metronomic photodynamic therapy as a new paradigm for photodynamic therapy: rationale and preclinical evaluation of technical feasibility for treating malignant brain tumors," *Photochem. Photobiol.* **80**(1), 22–30 (2004).
6. A. Bogaards, A. Varma, K. Zhang, D. Zach, S. K. Bisland, E. H. Moriyama, L. Lilge, P. J. Muller, and B. C. Wilson, "Fluorescence image-guided brain tumour resection with adjuvant metronomic photodynamic therapy: pre-clinical model and technology development," *Photochem. Photobiol. Sci.* **4**(5), 438–442 (2005).
7. A. A. Neves and K. M. Brindle, "Assessing responses to cancer therapy using molecular imaging," *Biochim. Biophys. Acta* **1766**(2), 242–261 (2006).
8. J. Narula, E. R. Acio, N. Narula, L. E. Samuels, B. Fyfe, D. Wood, J. M. Fitzpatrick, P. N. Raghunath, J. E. Tomaszewski, C. Kelly, N. Steinmetz, A. Green, J. F. Tait, J. Leppo, F. G. Blankenberg, D. Jain, and H. W. Strauss, "Annexin-V imaging for noninvasive detection of cardiac allograft rejection," *Nat. Med.* **7**(12), 1347–1352 (2001).
9. K. J. Yagle, J. F. Eary, J. F. Tait, J. R. Grierson, J. M. Link, B. Lewellen, D. F. Gibson, and K. A. Krohn, "Evaluation of 18F-annexin V as a PET imaging agent in an animal model of apoptosis," *J. Nucl. Med.* **46**(4), 658–666 (2005).
10. E. A. Schellenberger, A. Bogdanov, Jr., D. Hogemann, J. Tait, R. Weissleder, and L. Josephson, "Annexin V-CLIO: a nanoparticle for detecting apoptosis by MRI," *Mol. Imaging* **1**(2), 102–107 (2002).

11. C. Bremer, V. Ntziachristos, and R. Weissleder, "Optical-based molecular imaging: contrast agents and potential medical applications," *Eur. Radiol.* **13**(2), 231–243 (2003).
12. B. Laxman, D. E. Hall, M. S. Bhojani, D. A. Hamstra, T. L. Chenevert, B. D. Ross, and A. Rehemtulla, "Noninvasive real-time imaging of apoptosis," *Proc. Natl. Acad. Sci. U.S.A.* **99**(26), 16551–16555 (2002).
13. G. J. Czarnota, M. C. Kolios, J. Abraham, M. Portnoy, F. P. Ottensmeyer, J. W. Hunt, and M. D. Sherar, "Ultrasound imaging of apoptosis: high-resolution non-invasive monitoring of programmed cell death *in vitro*, *in situ* and *in vivo*," *Br. J. Cancer* **81**(3), 520–527 (1999).
14. D. A. Hamstra, T. L. Chenevert, B. A. Moffat, T. D. Johnson, C. R. Meyer, S. K. Mukherji, D. J. Quint, S. S. Gebarski, X. Fan, C. I. Tsien, T. S. Lawrence, L. Junck, A. Rehemtulla, and B. D. Ross, "Evaluation of the functional diffusion map as an early biomarker of time-to-progression and overall survival in high-grade glioma," *Proc. Natl. Acad. Sci. U.S.A.* **102**(46), 16759–16764 (2005).
15. B. A. Moffat, T. L. Chenevert, T. S. Lawrence, C. R. Meyer, T. D. Johnson, Q. Dong, C. Tsien, S. Mukherji, D. J. Quint, S. S. Gebarski, P. L. Robertson, L. R. Junck, A. Rehemtulla, and B. D. Ross, "Functional diffusion map: a noninvasive MRI biomarker for early stratification of clinical brain tumor response," *Proc. Natl. Acad. Sci. U.S.A.* **102**(15), 5524–5529 (2005).
16. B. Chance, P. Cohen, F. Jobsis, and B. Schoener, "Intracellular oxidation-reduction states *in vivo*," *Science* **137**, 499–508 (1962).
17. Z. Zhang, D. Blessington, H. Li, T. M. Busch, J. Glickson, Q. Luo, B. Chance, and G. Zheng, "Redox ratio of mitochondria as an indicator for the response of photodynamic therapy," *J. Biomed. Opt.* **9**(4), 772–778 (2004).
18. J. M. Reyes, S. Fermanian, F. Yang, S. Y. Zhou, S. Herretes, D. B. Murphy, J. H. Elisseeff, and R. S. Chuck, "Metabolic changes in mesenchymal stem cells in osteogenic medium measured by autofluorescence spectroscopy," *Stem Cells* **24**(5), 1213–1217 (2006).
19. D. K. Bird, L. Yan, K. M. Vrotsos, K. W. Eliceiri, E. M. Vaughan, P. J. Keely, J. G. White, and N. Ramanujam, "Metabolic mapping of MCF10A human breast cells via multiphoton fluorescence lifetime imaging of the coenzyme NADH," *Cancer Res.* **65**(19), 8766–8773 (2005).
20. Y. Wu, W. Zheng, and J. Y. Qu, "Sensing cell metabolism by time-resolved autofluorescence," *Opt. Lett.* **31**(21), 3122–3124 (2006).
21. M. Wakita, G. Nishimura, and M. Tamura, "Some characteristics of the fluorescence lifetime of reduced pyridine nucleotides in isolated mitochondria, isolated hepatocytes, and perfused rat liver *in situ*," *J. Biochem. (Tokyo)* **118**(6), 1151–1160 (1995).
22. J. R. Lakowicz, H. Szmacinski, K. Nowaczyk, and M. L. Johnson, "Fluorescence lifetime imaging of free and protein-bound NADH," *Proc. Natl. Acad. Sci. U.S.A.* **89**(4), 1271–1275 (1992).
23. H. Schneckenburger, M. Wagner, P. Weber, W. S. Strauss, and R. Sailer, "Autofluorescence lifetime imaging of cultivated cells using a UV picosecond laser diode," *J. Fluoresc.* **14**(5), 649–654 (2004).
24. J. Yang, X. Liu, K. Bhalla, C. N. Kim, A. M. Ibrado, J. Cai, T. I. Peng, D. P. Jones, and X. Wang, "Prevention of apoptosis by Bcl-2: release of cytochrome *c* from mitochondria blocked," *Science* **275**(5303), 1129–1132 (1997).
25. J. Cai and D. P. Jones, "Superoxide in apoptosis. Mitochondrial generation triggered by cytochrome *c* loss," *J. Biol. Chem.* **273**(19), 11401–11404 (1998).
26. I. Kruman, Q. Guo, and M. P. Mattson, "Calcium and reactive oxygen species mediate staurosporine-induced mitochondrial dysfunction and apoptosis in PC12 cells," *J. Neurosci. Res.* **51**(3), 293–308 (1998).
27. E. Maeno, Y. Ishizaki, T. Kanaseki, A. Hazama, and Y. Okada, "Normotonic cell shrinkage because of disordered volume regulation is an early prerequisite to apoptosis," *Proc. Natl. Acad. Sci. U.S.A.* **97**(17), 9487–9492 (2000).
28. R. Bertrand, E. Solary, P. O'Connor, K. W. Kohn, and Y. Pommier, "Induction of a common pathway of apoptosis by staurosporine," *Exp. Cell Res.* **211**(2), 314–321 (1994).
29. E. Maeno, T. Shimizu, and Y. Okada, "Normotonic cell shrinkage induces apoptosis under extracellular low Cl conditions in human lymphoid and epithelial cells," *Acta Physiol. (Oxford)* **187**(1–2), 217–222 (2006).
30. S. Teramoto, T. Tomita, H. Matsui, E. Ohga, T. Matsuse, and Y. Ouchi, "Hydrogen peroxide-induced apoptosis and necrosis in human lung fibroblasts: protective roles of glutathione," *Jpn. J. Pharmacol.* **79**(1), 33–40 (1999).
31. B. Chance, B. Schoener, R. Oshino, F. Itshak, and Y. Nakase, "Oxidation-reduction ratio studies of mitochondria in freeze-trapped samples. NADH and flavoprotein fluorescence signals," *J. Biol. Chem.* **254**(11), 4764–4771 (1979).
32. C. Y. Liu, C. F. Lee, and Y. H. Wei, "Quantitative effect of 4977 bp deletion of mitochondrial DNA on the susceptibility of human cells to UV-induced apoptosis," *Mitochondrion* **7**(1–2), 89–95 (2007).
33. C. Y. Liu, C. F. Lee, C. H. Hong, and Y. H. Wei, "Mitochondrial DNA mutation and depletion increase the susceptibility of human cells to apoptosis," *Ann. N.Y. Acad. Sci.* **1011**, 133–145 (2004).
34. V. Ghukasyan, Y.-Y. Hsu, S.-H. Kung, and F.-J. Kao, "Application of fluorescence resonance energy transfer resolved by fluorescence lifetime imaging microscopy for the detection of enterovirus 71 infection in cells," *J. Biomed. Opt.* **12**(2), 024016 (2007).
35. S. Huang, A. A. Heikal, and W. W. Webb, "Two-photon fluorescence spectroscopy and microscopy of NAD(P)H and flavoprotein," *Biophys. J.* **82**(5), 2811–2825 (2002).
36. I.-H. Chen, S.-W. Chu, C.-K. Sun, P.-C. Cheng, and B.-L. Lin, "Wavelength dependent damage in biological multi-photon confocal microscopy," *Opt. Quantum Electron.* **34**(12), 1251–1266 (2002).
37. J. R. Lakowicz, *Principles of Fluorescence Spectroscopy*, Kluwer Academic/Plenum, New York (1999).
38. L. Michea, C. Combs, P. Andrews, N. Dmitrieva, and M. B. Burg, "Mitochondrial dysfunction is an early event in high-NaCl-induced apoptosis of mIMCD3 cells," *Am. J. Physiol. Renal. Physiol.* **282**(6), F981–F990 (2002).
39. H. D. Vishwasrao, A. A. Heikal, K. A. Kasischke, and W. W. Webb, "Conformational dependence of intracellular NADH on metabolic state revealed by associated fluorescence anisotropy," *J. Biol. Chem.* **280**(26), 25119–25126 (2005).
40. A. Gafni and L. Brand, "Fluorescence decay studies of reduced nicotinamide adenine dinucleotide in solution and bound to liver alcohol dehydrogenase," *Biochemistry* **15**(15), 3165–3171 (1976).
41. A. Visser and A. van Hoek, "The fluorescence decay of reduced nicotinamides in aqueous solution after excitation with UV mode locked Ar ion laser," *Photochem. Photobiol.* **33**, 35–40 (1981).
42. L. K. Klaidman, A. C. Leung, and J. D. Adams, Jr., "High-performance liquid chromatography analysis of oxidized and reduced pyridine dinucleotides in specific brain regions," *Anal. Biochem.* **228**(2), 312–317 (1995).
43. Y. Avi-Dor, J. M. Olson, M. D. Doherty, and N. O. Kaplan, "Fluorescence of pyridine nucleotides in mitochondria," *J. Biol. Chem.* **237**, 2377–2383 (1962).
44. M. C. Skala, K. M. Riching, D. K. Bird, A. Gendron-Fitzpatrick, J. Eickhoff, K. W. Eliceiri, P. J. Keely, and N. Ramanujam, "*In vivo* multiphoton fluorescence lifetime imaging of protein-bound and free nicotinamide adenine dinucleotide in normal and precancerous epithelia," *J. Biomed. Opt.* **12**(2), 024014 (2007).
45. J. M. Levitt, A. Baldwin, A. Papadakis, S. Puri, J. Xylas, K. Munger, and I. Georgakoudi, "Intrinsic fluorescence and redox changes associated with apoptosis of primary human epithelial cells," *J. Biomed. Opt.* **11**(6), 064012 (2006).
46. J. Liang, W. L. Wu, Z. H. Liu, Y. J. Mei, R. X. Cai, and P. Shen, "Study the oxidative injury of yeast cells by NADH autofluorescence," *Spectrochim. Acta, Part A* **67**(2), 355–359 (2007).
47. L. Troiano, R. Ferraresi, E. Lugli, E. Nemes, E. Roat, M. Nasi, M. Pinti, and A. Cossarizza, "Multiparametric analysis of cells with different mitochondrial membrane potential during apoptosis by polychromatic flow cytometry," *Nat. Protoc.* **2**(11), 2719–2727 (2007).
48. E. Lugli, L. Troiano, R. Ferraresi, E. Roat, N. Prada, M. Nasi, M. Pinti, E. L. Cooper, and A. Cossarizza, "Characterization of cells with different mitochondrial membrane potential during apoptosis," *Cytometry, Part A* **68**(1), 28–35 (2005).
49. A. P. Halestrap, S. J. Clarke, and S. A. Javadov, "Mitochondrial permeability transition pore opening during myocardial reperfusion—a target for cardioprotection," *Cardiovasc. Res.* **61**(3), 372–385 (2004).
50. A. Halestrap, "Biochemistry: a pore way to die," *Nature (London)* **434**(7033), 578–579 (2005).
51. M. V. Zamaraeva, R. Z. Sabirov, E. Maeno, Y. Ando-Akatsuka, S. V. Bessonova, and Y. Okada, "Cells die with increased cytosolic ATP during apoptosis: a bioluminescence study with intracellular luciferase," *Cell Death Differ* **12**(11), 1390–1397 (2005).